Adhesion of high performance thermoplastic composites: Development of a bench and procedure for kinetics identification

Julien Avenet, Arthur Levy, Jean-Luc Bailleul, Steven Le Corre, Jérôme Delmas

Adhesion of high performance thermoplastic composites: development of a bench and procedure for kinetics identification

Julien Avenet[a,b], Arthur Levy[a,*], Jean-Luc Bailleul[a], Steven Le Corre[a], Jerôme Delmas[a]

[a] *Université de Nantes, CNRS, Laboratoire de thermique et énergie de Nantes, LTeN, UMR 6607, F-44000 Nantes, France.*
[b] *IRT Jules Verne, Chemin du Chaffault, 44340 Bouguenais, France*

Abstract

Thermoplastic welding, tape placement, 3D printing, overmoulding or even thermostamping involve adhesion of thermoplastic polymer at high temperature. Build-up of the mechanical resistance between two substrates is usually assumed to be driven by the diffusion of macromolecules at the interface, called healing phenomenon. Moreover, in continuous processes, such as some used in manufacturing of composites for aerospace structures, cycles are very short. Thus, there is a need for quantifying the adhesion of such materials especially when processed for short durations. With this aim, a temperature and pressure controlled welding bench was designed to enable the welding of double cantilever beam samples for short time (down to 1s). Adhesion of a carbon/PEKK composite was characterized over a wide range of residence times ranging from 1 second to 1 hour. Three bonding regimes were observed, corresponding to different stages of the adhesion build-up at the interface. Finally, the healing kinetics was identified.

Keywords: A. Thermoplastic resin, B. Adhesion, D. Mechanical testing, E. Assembly

1. Introduction

Thermoplastic matrix composites have gained popularity over recent decades partly because they do not require lengthy curing cycles, thus speeding their processing. Moreover, the ability to melt the matrix has led to many new forming and assembling processes, including thermo-forming, automated tape

*Corresponding author
Email addresses: julien.avenet@univ-nantes.fr (Julien Avenet), arthur.levy@univ-nantes.fr (Arthur Levy), jean-luc.bailleul@univ-nantes.fr (Jean-Luc Bailleul), steven.le-corre@univ-nantes.fr (Steven Le Corre), jerome.delmas@univ-nantes.fr (Jerôme Delmas)

placement, 3D-printing, pultrusion or welding processes such as ultrasonic or induction welding. In order to ensure good final quality, all these processes require heating and consolidation steps. Depending on authors, the word *consolidation* can refer to several different mechanisms: reduction of voids to fulfill allowable porosity levels [1–3], minimization of internal stresses [4] or maximization of the final crystallinity [5]. In this paper, we focus on the adhesion between plies [6–8] or between two composite parts in welding processes [5, 9–11]. The difference with the previously described consolidation phenomenon is that in our case we are interested in the interfacial consolidation between the coupons which we will refer to as adhesion. The autohesion phenomenon [12, 13] of the thermoplastic matrix is indeed a crucial mechanism that needs to be controlled in order to ensure sufficient end-quality of the welds.

Adhesion of thermoplastics, and more specifically thermoplastic composites, has been investigated for years. To enable adhesion, the composite substrates are pressed together for a certain time above the processing temperature of the polymer matrix. Several phenomena then lead to a build-up of strength at the interface [5, 14, 15]. Wool and O'Connor [12] described the adhesion process as a succession of five steps: (1) surface rearrangement, (2) surface approach, (3) wetting, (4) diffusion and (5) randomization. During the first two stages, the assembly has no mechanical strength as the initial interface still exists. First, deformation of the surface roughness, driven by the contact pressure and wetting, is required to ensure contact at the microscopic scale. This is the so-called *intimate contact*, which has been studied and modelled by several authors in various manufacturing processes. Once intimate contact is achieved, the interface gradually disappears through a *healing process* (steps (4) & (5)), and the mechanical strength at the interface develops to finally approach that of the bulk.

Contact between two substrates is not immediately perfect because of surface roughness. The concept of intimate contact was introduced to take into account the initial roughness of the surfaces and the evolution of physical contact between the substrates. Dara and Loos [16] first introduced the degree of intimate contact D_{ic}, which increases to 1 for full contact. Dara and Loos' model was then simplified by Lee and Springer [1] who modelled the surface as a succession of identical rectangles that spread under temperature and pressure loading. Some attempts were made to improve this geometrical description, *e.g.* Yang and Pitchumani [17]. All these models of the degree of intimate contact use a characteristic intimate contact time t_{ic} [1]:

$$t_{ic} \sim \frac{\mu(T)}{P} \tag{1}$$

where P is the closing pressure applied between the adherends and $\mu(T)$ is an effective temperature-dependent viscosity of either the polymer or the composite blend.

Once intimate contact is established, the macromolecules are free to move across the interface through the inter-diffusion process, which is also called autohesion in the case of two similar composite parts. This motion is usually

described by de Gennes reptation theory [18] where a molecular chain is considered as though confined in a tube representing the topological constraints due to neighboring chains, which prohibits lateral motions along the tube. Since the chain can only relax along the tube direction, the chain ends are free to move in any direction away from the tube so that the memory of the initial conformation is gradually lost up to a time t_{rep}, called the reptation time, when the chain has completely forgotten its initial configuration. The degree of healing D_h is classically defined as the ratio of the interface strength σ to bulk strength σ_∞ and is thus written [1, 12, 16]:

$$D_h = \frac{\sigma}{\sigma_\infty} = \left(\frac{G_{IC}}{G_{IC,\infty}} \right)^{1/2} \tag{2}$$

where $G_{IC,\infty}$ is the bulk fracture energy.

Some authors [19–21] have different theories to relate the microscopic scale macromolecule diffusion to the macroscopic mechanical properties. All agree that the fracture energy G_{IC} of the interface increases with the square root of time. Wool and O'Connor [12] showed that when the reptation time approaches, diffusion and randomization stages are completed and the maximum mechanical strength of the interface is reached. For long macromolecules, the full mechanical strength may be reached even for partial chain diffusion. Some authors [12, 21–23] therefore suggest to define the welding time $t_{w,\infty}$ required to reach the maximum mechanical strength of the interface. Thus this welding time $t_{w,\infty}$ is lower than the reptation time t_{rep} and

$$D_h = \left(\frac{t}{t_{w,\infty}} \right)^{1/4}, \tag{3}$$

can be adopted for isothermal conditions.

Within the scope of composite manufacturing process modelling, the above law of evolution can classically be extended to anisothermal temperature cycles [1, 24, 25]. One then needs to integrate the degree of healing rate which is written:

$$\frac{d\left(D_h^4\right)}{dt} = \frac{1}{t_{w,\infty}} \tag{4}$$

This is a classical approach used in the modelling of several manufacturing processes, such as press forming or compression moulding [16, 26], tape placement processes [6, 7] or welding [27].

Welding processes and adhesion mechanisms are well understood for unreinforced thermoplastics, where the mechanical resistance of the welded parts approaches the bulk properties of the adherends. In the case of fibre reinforced thermoplastic composites, some issues may arise due to their manufacturing and to the simple presence of fibres, often at very high volume fractions:

- confinement effects due to the presence of fibres, especially the case at high fibre fractions where the mean distance between fibres is very low,

- low amount of matrix available to melt at the interface,
- high roughnesses, due to the fibrous structure, leading to very different intimate contact from neat polymers,
- internal stresses intrinsically present at different scales (fibres, fibre bundles or unidirectional plies) [4],
- thermal history, such as autoclave cycle, that can induce matrix changes, especially for high performance composites that are processed at high temperature [28, 29]; it can also generate additional internal stresses likely to influence the adhesion values.

Overall, adhesion theories have been well experimentally validated for long residence times, ranging from a few minutes to a few days [1, 16, 24, 30]. However, composite forming processes are becoming faster and faster (some are even continuous) and the adhesion step is expected to be as short as possible, with residence time around a few seconds as shown in Fig. 1. A proper characterization of the mechanical bond between adherends for such short residence times is, therefore, very relevant to understanding and controlling the rapid processes used in the industry.

The first section of this paper presents the materials and the experimental approach developed in this work, including the design of a new laboratory scale bench dedicated to the study of composite adhesion kinetics at short residence time by the means of a stopped welding experiment. The second section validates this novel procedure. In the last section, results for an industrial aeronautical grade thermoplastic composite are presented. The obtained bonding kinetics is identified and compared with existing results on longer residence times.

2. Experimental methods

This section describes the adhesion characterization procedure. Thermoplastic composite laminate coupons were welded together using the welding bench. The adhesion was then assessed using a double cantilever mechanical test following the ASTM standard [31].

2.1. Material

The material used in this study was an aeronautical grade Arkema PEKK 7002 thermoplastic reinforced with carbon fibres. Laminates consisted of 12 plies of symmetric unidirectional fibre layup of [0°/90°]. Samples were hand laid-up into a flat plate. On one of the surfaces, a 50 µm thick film of neat PEKK polymer, shown in Fig. 2, was applied to ease the welding process. The layup was then consolidated in an autoclave at 380°C for 2 hours. The melting temperature of this material ranged from 300°C to 350°C, with a melting peak temperature of 330°C. The crystallization kinetics of the PEKK 7002 matrix was investigated by Choupin et al. [32] and found to be rather slow compared

to other high performance thermoplastics: the matrix is partially amorphized at a cooling rate of 20°C/min and completely quenched at 50°C/min.

The manufacturer recommends processing at a temperature above 350°C. It has been shown degradation can occur at such temperatures, associated with chemical modification [28, 29], which likely influences the welding time, as discussed below.

Before the welding experiments, the 2.3 mm thick composite plates were cut into 125 x 25 mm samples (Fig. 3) using a Protomax waterjet cutting machine. A countersunk hole was machined in each sample 10 mm from one end to insert a loading pin used for gripping the sample during the fracture test. The coupons were then manually cleaned using acetone solvent and dried in a vacuum chamber at 180°C for 20 hours in order to remove residual water and limit the laminate deconsolidation phenomenon that would occur during the welding sequence.

The side of the composite that would be in contact with the mold was covered with polyimide tape to facilitate the removal of the welded coupons after the welding procedure. The initial crack between the two composite adherends was created by inserting a non-adhesive 20 µm thick aluminum foil between the two samples at 50 mm from the load application point such that the welded area was 65 mm long by 25 mm wide, matching the ASTM D5528 standard. Finally, the loading pins were inserted into the samples prior to the welding experiment. They were engaged in a cavity machined inside the mold as described in the next section.

2.2. Experimental welding bench

The welding bench was developed for welding composite substrates for a finite amount of time (down to a few seconds) and under constant isothermal conditions. The TACOMA (for Thermo-Adhesion by COnductive heating of composite MAterials) setup is shown in Fig. 4.

Design. The mold comprises two L-shaped copper symmetric platens. One is static and the other moving. Their dimension is the same as that of the samples, *i.e.* the width b is 25 mm and the length L 125 mm. Thus, the entire lengths of the samples are heated and pressed together. Additionally two lateral copper plates (one on each side of the mold) are fastened on the mold to separate the cavity from the ambient air and ensure a confined cavity. In order to avoid holding issues of the samples [33], the setup was designed with the moving platen sliding horizontally. Thus, the samples are simply positioned vertically on each platen, facing each other and resting on their sides. Thanks to the lateral plates, the static platen acts as a die and the moving platen as a punch. Finally, a slider is attached to the insulating material of the sliding platen to control the shear edge gap and bear the weight of the platen.

Temperature control. Control thermocouples are embedded inside the copper platens near the sample surfaces (1 mm from the surface). The platens are

heated with heating cartridges. Additionally, two internal channels were machined in each platen in order to allow fast and spatially homogeneous water cooling of the copper mold, thus making it possible to quench the samples and perform stopped experiments.

Pressure control. The moving platen is attached in series to a pneumatic piston, a load cell and an insulating material to protect the load cell from the high temperatures and to limit heat losses. The 80 mm diameter pneumatic piston uses compressed air with a maximum entry pressure of 6 bars, which results in a maximum force of 5 kN corresponding to a maximum effective pressure on the samples of about 10 bars. The force is recorded with a 10 kN load cell.

Synchronisation. The temperature PID controller, piston pressure application and water quenching are all controlled automatically via a homemade Labview interface. Temperatures and forces are also acquired in Labview every 0.5 s. The whole procedure is written in one integrated program, ensuring synchronisation.

Protocol. The experimental protocol to weld the two composite coupons is illustrated in Fig. 5. After positioning the two substrates in the mold with a platen open to ensure a separation gap, the procedure can be divided into five steps:

1. heating of the copper block from room temperature up to a temperature higher than the melting temperature of the material (at first the two samples are not in contact and the matrix-rich surfaces are facing each other),
2. homogenization of the temperature at the surface of the coupons for a dwell time t_{dwell},
3. once the setpoint temperature is reached and homogeneous inside the mold, pressure is applied with the pneumatic piston to weld the samples during a defined contact time t_c,
4. fast cooling of the setup with water circulation to stop the welding process and
5. the pressure is released.

2.3. Double Cantilever Beam (DCB) fracture test

The mechanical strength of the welded interface was assessed using a double cantilever beam (DCB) fracture test following the ASTM D5528 standard [31]. The welded samples were mounted on a 100 kN Zwick Roell tensile machine and homemade sample holders were used to fix the loading pins onto the machine grips. Tests were performed in displacement control mode with a constant displacement rate v of 1 mm.min^{-1}, which corresponds to a quasi-static condition. The pins were designed and machined to minimize unwanted torque in the load (see Fig. 6). The pins did not, in fact, conform to the ASTM standard which suggests bonded systems. Nevertheless their design prevented failure between the sample and the pins since they were directly inserted into the sample. Furthermore, they were well centred in the sample width, which prevented torsion phenomena.

The load and displacement were continuously recorded during the test. Intrinsically, due to the nature of DCB tests on composite plates, the lever arm between the application point and the welded area generates bending inside both composite plates, which results in some elastic energy storage.

The mode I strain energy release rate also called interlaminar fracture toughness is defined as the energy necessary to propagate a crack over a unit surface. For an elastic linear structure, the analysis of a double cantilever beam test is based on the change of compliance. The growth of a crack from a to $a + \Delta a$ induces a change in the compliance, resulting in a loss of the stored energy. In this method, the compliance is determined using standard Euler-Bernoulli beam theory, which considers that the adherents are cantilevered at the crack tip. It is then possible to determine the interlaminar fracture toughness from the Irwin-Kies equation [34]:

$$G_I = \frac{P^2}{2b}\frac{\partial C}{\partial a} \tag{5}$$

where b is the width of the samples, P is the applied force. The compliance $C = \delta/P$ and the displacement δ at the loading point, according to Euler-Bernoulli beam theory are respectively:

$$C = \frac{8a^3}{Ebh^3} \qquad \delta = \frac{2Pa^3}{3EI} \tag{6}$$

where h is the thickness, E is the Young modulus and $I = bh^3/12$ is the moment of inertia of the beam.

The derivation of Eq. (6) and substitution in (5) gives the most frequently used expressions of the mode I interlaminar fracture toughness [31, 35]:

$$G_I = \frac{3P\delta F}{2ba} \tag{7}$$

where F is a correction factor accounting for large displacement effects [31], *i.e.* shortening of the moment arm and tilting of the loading pins. This factor is strongly dependent on the sample and pin geometry and clamping stiffness.

2.4. Test matrix

Welding tests were carried out for three different temperatures above the melting temperature of the polymer matrix: 355, 370 and 380°C, and for various contact times from 1 second to 1 hour, as detailed in Table 1. At least three replicates were performed for each contact time at 355°C and 380°C. These two temperatures were thoroughly investigated whereas less data points were tested for 370°C.

3. Procedure validation

The adhesion characterization procedure consisted of the stopped welding experiment in the TACOMA bench followed by a DCB test to assess bonding

quality. In this section, temperature homogeneity and quenching quality in the TACOMA bench are first discussed. We then cover how the DCB test is then validated.

3.1. Thermal management

Temperature homogeneity inside the TACOMA setup was first characterized by placing a type K thermocouple at different locations between the two copper platens of the mold without any samples, such that the thermocouple did not touch the mold. These tests were performed with and without the two lateral copper plates described in section 2.2.

Samples instrumented with 80 µm type K thermocouples were also tested in the TACOMA setup. The thermocouples were embedded on the matrix-rich layer of samples, at locations given in Table. 2, in order to record the temperature at the interface between the two samples during the welding sequence. The sequence consisted in heating to 380°C, followed by 100 seconds contact.

Fig. 7 shows the evolution of the temperature at the interface between the two samples at different positions during the welding sequence. At first, the characteristic cooling rates in the mold and at the sample interface (at position T4) are $20°C.s^{-1}$ and $12°C.s^{-1}$, respectively. This confirms that the sample was quenched. According to the crystallization kinetics identified by Choupin et al. [32], the sample is completely amorphous. This validates the rapid stopping of the healing process. This test, therefore, allows the determination of the time needed for the targeted temperature at the interface to be reached, which occurs during the heating phase. The lateral plates indeed prevent natural air convection in the cavity. In order to perform an isothermal welding cycle, the pressure must be applied once the interface has reached the targeted temperature. For a welding temperature of 380°C, the dwell time is about 300 seconds.

The test also provided information on edge effect. Indeed, samples are positioned against the copper mold. All faces of the sample except the one that will be welded are in contact with the copper. Therefore, a 3D temperature gradient develops in the samples and leads to gradients in degree of adhesion. The instrumentation of the sample along its width validated that edge effects are present on the sides. For instance, in Fig. 7, heating and cooling rates are faster for thermocouple T3. The edge effects are crucial during the cooling phase since they might induce a healing degree profile along the width of the sample: the centre of the sample stays at a high temperature for longer before the cooling starts. The iso degree of adhesion along the sample width could therefore present a profile that is not straight. Nonetheless, as discussed in the following section, the adhesion gained during cooling was negligible compared with that gained during the contact phase under isothermal conditions.

3.2. DCB validation

The load-displacement curves obtained from the double cantilever beam fracture tests are presented in Fig. 8. They present a saw-tooth behaviour characterized by sudden drops in the recorded force that correspond to unstable

fractures. This is known as stick-slip crack growth [36] accompanied by high-speed propagation and arrest. In contrast, stable behaviour is characterized by continuous crack growth with increasing displacement. This phenomenon has been observed by different authors. Harkous et al. [33] attributed it to very rapid failure of the welded area and explained that, for high resistance composite, the large amount of energy released causes a long propagation of the crack and, consequently, a complete breaking of the part. Sacchetti et al. [37] also observed this unstable behaviour for unidirectional Carbon/PEEK laminates and explained that it was due to a non-uniformity of the matrix rich layer at the surface of their samples, resulting in a non-uniform interlaminar fracture toughness along the crack path.

Due to unstable crack propagation and difficulties in measuring crack length during the double cantilever beam test, interlaminar fracture toughness G_{IC} can be calculated at the crack initiation point, corresponding to the first peak in the load-displacement curve. At this point, the crack length is known and corresponds to the length a_0 of the non-adhesive aluminum insert. These $G_{IC,ini}$ values are calculated using Eq. (7).

In order to confirm the relevance of this $G_{IC,ini}$ value, incremental DCB tests were performed. This consisted in positioning a clamp at different positions along the sample length to stop crack propagation and performing a DCB test. Once the crack had propagated from its initial length to the one corresponding to the clamp position, the samples were unloaded at 25 mm.min^{-1}, the clamp was moved to a further position and the samples were reloaded at 1 mm.min^{-1}. This allowed the calculation of G_{IC} at each position of the clamp, corresponding to different known crack lengths. The load-displacement curves corresponding to these tests are presented in Fig. 9. The propagation of the crack remained unstable between two locations of the clamp, characterized by a sudden force drop. G_{IC} values were calculated as before using Eq. (7), with a being the location of the clamp from the loading application point, in this case successively 55, 60, 65 and 75 mm. The first value corresponds to the crack initiation $G_{IC,ini}$ while the other values are associated with crack propagation and can be written as $G_{IC,prop}$. As visible from Fig. 9, incremental curves sometimes exhibit a slight non-linearity before the next propagation of the crack. This can be attributed to the fact that the clamp might not perfectly stop the crack propagation leading to a more disturbed crack front for the next clamp position. This leads in turn to this observed change of compliance. Evolution of G_{IC} values versus crack length is plotted in Fig. 10 for three different welding times. This incremental test is particularly useful for samples welded for very short residence times, due to low fracture resistance and heterogeneity along the total welded length. In practice, it was only used for low adhesion situations.

The repeatability of the classical DCB tests shows a 15 % error on $G_{IC,ini}$ measurement. This 15 % error was applied to the first point of the incremental DCB test. In Fig. 10 the hatched area corresponds to this error measurement interval and the dotted line to $G_{IC,ini}$ value. Overall, the $G_{IC,porp}$ obtained from incremental DCB tests all fall within this interval. For our material, this validates that the energy release rate for crack propagation equates that for

initiation. Thus, $G_{IC,ini}$ will be used in the following the initiation values.

4. Results and discussion

In this section, the characterization methodology described above is applied to the Carbon-PEKK material. The experimental campaign described in section 2.4 and Table 1 is followed.

4.1. Bonding regimes

Interlaminar fracture toughness of the samples welded at different temperatures are plotted against contact time in Fig. 11, where three adhesion regimes can be identified. Micropgraphs and SEM images of the interfaces corresponding to these respective regimes are visible in Figure 12.

The first regime corresponds to a short residence time during which intimate contact is not completed. Air gaps are visible at the welded interface in Fig. 12. Contact is probably achieved only at a few spots where healing has started. Healing is also probably incomplete at those contact points, which results in overall poor bonding energies as evidenced by the SEM images in Fig. 12. It should be remembered that for this TACOMA test, the closing pressure is fairly high (3.2 bars) and thus ensures rapid intimate contact compared with the healing phenomenon, as clearly seen in Fig. 11.

The second regime starts when intimate contact is fully achieved on the whole surface and the evolution of bonding energy is only due to healing. This regime will be discussed in the next section and used for healing kinetics identification. The micrograph in Fig. 12 reveals a residual matrix-rich layer at the interface. The SEM image shows matrix deformation indicating that the fracture is mostly cohesive. Adhesion is polymer autohesion.

Finally, in the terminal regime, the fracture energy is still increasing with time. The cross-section shows that the resin-rich layer has disappeared due to fibre motion and resin bleed. This stage is characterized by a competition between matrix cohesive bonding and other adhesion phenomena such as fibre bridging combined with differential flow and segregation of the polymer matrix, as seen sparsely in Fig. 12. Such phenomena lead to higher values of G_{IC} and are thus not associated with autohesion healing process through macromolecule reptation. In addition, these values present a strong standard deviation due to the non-repeatability in the occurrence of these phenomena. Such observations of fibre bridging have been reported in the literature [38, 39] but, as mentioned by Sacchetti et al. [37], these studies were based on typical consolidation techniques such as hot plate pressing or autoclave manufacturing, characterized by long residence time that allow the fibres to migrate at the interface. In the case of welding for a short residence time, fibre bridging is expected to be reduced, especially with the presence of a matrix-rich region at the interface. In our case, the observed fibre bridging can be related to these consolidation studies since it only occurs at long welding time. Thus, this validates that the corresponding bonding energies are part of a third regime where healing is already complete.

G_{IC} values can be seen to reach a small plateau at the end of the second regime. $G_{IC,\infty}$ was calculated as the mean value of G_{IC} measured on this plateau and is equal to $2.3 \pm 0.1\ kJ.m^{-2}$. It corresponds to the maximum mode I interlaminar fracture toughness of fully healed samples, *i.e.* to $D_h = 1$. Values of mode I interlaminar fracture toughness G_{IC} might seem high compared with values for high performance polymers found in the literature. This is explained by the TACOMA welding process cycle. At such a high cooling rate, the matrix is completely amorphous [32], thus leading to a high ductility compared with semi-crystalline state. It results in a high plastic deformation of the matrix as demonstrated by Sacchetti et al. [40] for carbon/PPS unidirectional laminates, thus increasing the interlaminar fracture toughness compared to crystallized parts. Similar high values were reported for unidirectional carbon/PEEK laminates by Sacchetti et al. [37] who demonstrated that matrix plastic deformation indeed induces an increase of G_{IC} values.

4.2. Healing identification

The raw data corresponding to regime II in the previous section were used to characterize the welding time for the healing mechanism. Degree of healing was calculated using the classical law in Eq. (2) where $G_{IC,\infty}$ is the one determined in the previous section and is plotted versus the fourth root of the contact time in Fig. 13. Since healing kinetics was identified on the second regime, the first data points, corresponding to the first coupled regime, are discarded from the linear fit, and the curves do not intersect the origin. The welding times are directly identified from the slope of the linear fit in Fig. 13, which is equal to $1/t^4_{w,\infty}$ according to Eq. (3). The welding times for the three isothermal temperatures are given in Table. 3.

The laminates used in this study were consolidated for 2 hours in an autoclave at 380°C. At these temperatures it has been shown that degradation associated with chemical modification can occur [28, 29], thus increasing the relaxation time. The identified welding time was consequently increased, explaining the large values – of a magnitude of one hundred seconds – that are obtained.

The welding time was fitted to a temperature dependant Arrhenius relationship:

$$t_{w,\infty}(T) = A \exp\left(\frac{E_a}{RT}\right) \tag{8}$$

where E_a is the activation energy and A the pre-exponential factor. These parameters could be determined for our composite using the Arrhenius plot given in Fig. 14. The pre-exponential factor obtained was $A = 3,01.10^{-3}\ s$ and the activation energy $E_a = 55,5\ kJ.mol^{-1}$. The degree of healing could now be computed by integrating the degree of healing rate (4) substituting the identified healing kinetics Eq. (8) for any industrial temperature history.

5. Conclusion

In this work, adhesion of high performance thermoplastic composites was investigated. Besides the intimate contact phenomenon that may limit adhesion when rough surfaces are welded or limited pressure is used, healing is the main phenomenon controlling the bonding quality. The objective was to characterize adhesion for conditions close to the industrial process, especially short residence time.

A novel instrumented laboratory scale welding bench was developed to weld composite substrates for controlled contact times and under controlled constant pressure and isothermal conditions. The lower time limit of this bench is 1 second, due to inertia of the piston, and the upper pressure limit onto the samples is about 10 bars. Instrumented samples were used to validate the thermal homogeneity of the bench and the characteristic cooling rates it enabled at both the mold and the sample interfaces. Our device was shown to enable the quenching of our composite samples, thus proving the effectiveness of a stopped healing process.

The mechanical quality of the bonded substrates was assessed with a double cantilever beam test. Because composite samples systematically show unstable crack propagation, only the value of the interlaminar fracture toughness at the crack initiation was used in the analysis. Nevertheless, an original incremental DCB procedure was developed and was shown to give the same results as the initiation point method. By doing so, both procedures, which are therefore equivalent, were validated and the incremental DCB fracture test was proved to be of particular interest for the characterization of low adhesion energies, associated with short residence time.

Welding tests over a wide range of contact time were performed on a high performance thermoplastic composite. It was revealed that adhesion between two composite substrates develops following three successive regimes. The first regime is a coupled regime where intimate contact is not yet achieved. The second regime is purely associated with inter-diffusion of the chains, *i.e.* healing, where the healing degree evolves linearly with the fourth root of time. Finally, a third adhesion regime was found in our case. For longer welding times, other adhesion phenomena occurred such as fibre bridging and matrix segregation, leading to the bond strength to exceed the cohesive strength of the matrix. They are therefore not associated with pure healing. They imply motion of fibres that leads to a mechanical fastening, but probably also to unwanted microstructural changes. Healing kinetics were finally identified from a test campaign on three isothermal temperatures. For our carbon PEKK plates, the identified welding time to complete the healing process is of the order of one hundred seconds, which can be attributed to thermal aging during autoclave pre-manufacturing of the samples.

This novel experimental welding bench can be used to characterize adhesion for residence time as short as a few seconds, under isothermal conditions. As a perspective for future research, investigations will be carried out at a shorter time scale to study the kinetics of intimate contact and then characterize and

model the whole adhesion process. To do this, further investigations will be needed to account for the transient thermal regime induced by the quenching and to separate the intimate contact from the healing contributions in this so-called *coupled regime*.

6. Acknowledgements

The authors would like to acknowledge the funding they received from the PERFORM project managed by IRT Jules Verne (French Institute for Research and Technology in Advanced Manufacturing Technologies for Composite, Metallic and Hybrid Structures), which made this work possible. The authors would like to associate the industrial partners of the PERFORM project: Airbus, Stelia Aerospace, Faurecia, Naval Group and Daher.

The authors would also like to thank Professor Erwan Verron for fruitful discussion about fracture mechanics. The bench design and manufacturing was initiated thanks to Thomas Cender to whom we are deeply grateful for his contribution. We thank Yannick Benoit from Ecole Centrale de Nantes for his help with the SEM images. Finally, the design and manufacturing would not have been possible without the help of Nicolas Lefevre.

References

[1] Woo Il Lee and George S. Springer. A Model of the Manufacturing Process of Thermoplastic Matrix Composites. *J. Compos. Mater.*, 21(11):1017–1055, 1987.

[2] Sridhar Ranganathan, Suresh G. Advani, and Mark A. Lamontia. A Non-Isothermal Process Model for Consolidation and Void Reduction during In-Situ Tow Placement of Thermoplastic Composites, 1995.

[3] John Tierney and John W. Gillespie. Modeling of Heat Transfer and Void Dynamics for the Thermoplastic Composite Tow-Placement Process. *J. Compos. Mater.*, 37(19):1745–1768, 2003.

[4] Patricia P. Parlevliet, Harald E.N. Bersee, and Adriaan Beukers. Residual stresses in thermoplastic composites - a study of the literature. Part I: Formation of residual stresses. *Compos. Part A Appl. Sci. Manuf.*, 38(6): 1581–1596, 2007.

[5] C. Ageorges and Y. Le. Fusion Bonding of Polymer Composites. In *Fusion Bond. Polym. Compos.* Springer-Verlag London, 2002.

[6] Fazil O. Sonmez and H. Thomas Hahn. Analysis of the on-line consolidation process in thermoplastic composite tape placement. *J. Thermoplast. Compos. Mater.*, 10(6):543–572, 1997.

[7] M. A. Khan, P. Mitschang, and R. Schledjewski. Parametric study on processing parameters and resulting part quality through thermoplastic tape placement process. *Journal of Composite Materials*, 47(4):485–499, 2012.

[8] W.J.B. Grouve, L.L. Warnet, B. Rietman, H.A. Visser, and R. Akkerman. Optimization of the tape placement process parameters for carbon-PPS composites. *Composites Part A: Applied Science and Manufacturing*, 50: 44–53, 2013.

[9] Arthur Levy, Dirk Heider, John Tierney, and John W. Gillespie. Inter-layer thermal contact resistance evolution with the degree of intimate contact in the processing of thermoplastic composite laminates. *J. Compos. Mater.*, 48(4):491–503, 2014.

[10] Francisco Sacchetti. *Interlaminar toughness of fusion bonded thermoplastic composites*. PhD thesis, University of Twente, Enschede, the Netherlands, 2017.

[11] H. Shi, Irene Fernandez Villegas, and Harald E.N. Bersee. Modelling of Heat Transfer and Consolidation for Thermoplastic Composites Resistance Welding. In *ICCM 18th Int. Conf. Compos. Mater.*, 2018.

[12] R. P. Wool and K. M. O'Connor. A theory of crack healing in polymers. *J. Appl. Phys.*, 52(10):5953–5963, 1981.

[13] Firas Awaja, Michael Gilbert, Georgina Kelly, Bronwyn Fox, and Paul J. Pigram. Adhesion of polymers. *Progress in Polymer Science*, 34(9):948–968, 2009.

[14] V. K. Stokes and S. Y. Hobbs. Strength and bonding mechanisms in vibration-welded polycarbonate to polyetherimide joints. *Polym. Eng. Sci.*, 29(23):1667–1676, 1989.

[15] David A Grewell, Avraham Benatar, and Joon B Park. *Plastics and Composites Welding Handbook*. Hanser, 2003.

[16] Philip H. Dara and Alfred C. Loos. Thermoplastic Matrix Composite Processing Model. Technical report, Virginia Tech - Center for Composite Materials and Structures, Blacksburg, Virginia, 1985.

[17] F. Yang and R. Pitchumani. A fractal Cantor set based description of interlaminar contact evolution during thermoplastic composites processing. *J. Mater. Sci.*, 36:4661–4671, 2001.

[18] P. G. De Gennes. Reptation of a polymer chain in the presence of fixed obstacles. *J. Chem. Phys.*, 55:571–579, 1971.

[19] K. Jud, H. H. Kausch, and J. G. Williams. Fracture Mechanics Studies of Crack Healing and Welding of Polymers. *J. Mater. Sci.*, 16:204–210, 1981.

[20] Stephen Prager and Matthew Tirrell. The healing process at polymer – polymer interfaces. *J. Chem. Phys.*, 75(10):5194–5198, 1981.

[21] Young Hwa Kim and Richard P. Wool. A theory of healing at a polymer-polymer interface. *Macromolecules*, 16:1115–1120, 1983.

[22] Richard P. Wool, B.-L. Yuan, and 0. J McGarel. Welding of Polymer Interfaces. *Polym. Eng. Sci.*, 29(19):1340–1367, 1989.

[23] F. Yang and R. Pitchumani. Interlaminar contact development during thermoplastic fusion bonding. *Polym. Eng. Sci.*, 2002.

[24] F. Yang and R. Pitchumani. Healing of thermoplastic polymers at an interface under nonisothermal conditions. *Macromolecules*, 35:3213–3224, 2002.

[25] C. Ageorges, L. Ye, and M. Hou. Advances in fusion bonding techniques for joining thermoplastic matrix composites: A review. *Compos. - Part A Appl. Sci. Manuf.*, 32(6):839–857, 2001.

[26] A. C. Loos and Min-Chung Li. Non-Isothermal Autohesion Model for Amorphous Thermoplastic Composites. *Journal of Thermoplastic Composite Materials*, 7(4):280–310, 1994.

[27] Arthur Levy, Steven Le Corre, and Irene Fernandez Villegas. Modeling of the heating phenomena in ultrasonic welding of thermoplastic composites with flat energy directors. *J. Mater. Process. Technol.*, 214(7):1361–1371, 2014.

[28] Tanguy Choupin, B. Fayolle, Gilles Régnier, C. Paris, J. Cinquin, and B. Brulé. Macromolecular Modifications of Poly (EtherKetoneKetone) (PEKK) Copolymer at the Melting State. *Polym. Degrad. Stab.*, 155:103–110, 2018.

[29] Thomas Cender, Arthur Levy, and Steven Le Corre. Continuous Fusion Bonding of High Temperatures Thermoplastic Composite Structures with Volumetric Heating. In *ICMAC Conf.*, Nottingham, 2018.

[30] S. S. Voyutskii and V. L. Vakula. The Role of Diffusion Phenomena in Polymer-to-Polymer Adhesion. *J. Appl. Polym. Sci.*, 7(2):475–491, 1963.

[31] ASTM International. D5528 - Standard Test Method for Mode I Interlaminar Fracture Toughness of Unidirectional Fiber-Reinforced Polymer Matrix Composites, 2013.

[32] T. Choupin, B. Fayolle, G. Régnier, C. Paris, J. Cinquin, and B. Brulé. Isothermal crystallization kinetic modeling of poly(etherketoneketone) (PEKK) copolymer. *Polym. (United Kingdom)*, 111:73–82, 2017.

[33] Ali Harkous, Tomasz Jurkowski, Jean Luc Bailleul, and Steven Le Corre. Influence of the temperature on the composites' fusion bonding quality. *AIP Conf. Proc.*, 1896(April), 2017.

[34] G. R. Irwin and J. A. Kies. Critical Energy Rate Anaysis of Fracture Strength. *Weld. J. Res. Suppl.*, 33:193–198, 1954.

[35] V. Tamuzs, S. Tarasovs, and U. Vilks. Delamination properties of translaminar-reinforced composites. *Compos. Sci. Technol.*, 63(10):1423–1431, 2003.

[36] T. W. Webb and Aifantis E. C. Crack Growth Resistance Curves and Stick-Slip Fracture Instabilities. *Mechanics Research Communication*, 24 (2):123–130, 1997.

[37] Francisco Sacchetti, Wouter J.B. Grouve, Laurent L Warnet, and Irene Fernandez Villegas. Effect of resin-rich bond line thickness and fibre migration on the toughness of unidirectional Carbon/PEEK joints. *Compos. Part A Appl. Sci. Manuf.*, 109:197–206, 2018.

[38] A.B. Pereira, A. B. De Morais, M. F. S. F. de Moura, and A.G. Magalhaes. Mode I interlaminar fracture of carbon epoxy laminates. *Compos. Part A Appl. Sci. Manuf.*, 91:1–8, 2016.

[39] Vikas Kaushik and Anup Ghosh. Experimental and numerical characterization of Mode I fracture in unidirectional CFRP laminated composite using XIGA-CZM approach. *Eng. Fract. Mech.*, 211(February):221–243, 2019.

[40] Francisco Sacchetti, Wouter J.B. Grouve, Laurent L Warnet, and Irene Fernandez Villegas. Effect of cooling rate on the interlaminar fracture toughness of unidirectional Carbon/PPS laminates. *Engineering Fracture Mechanics*, 203:126–136, 2018.

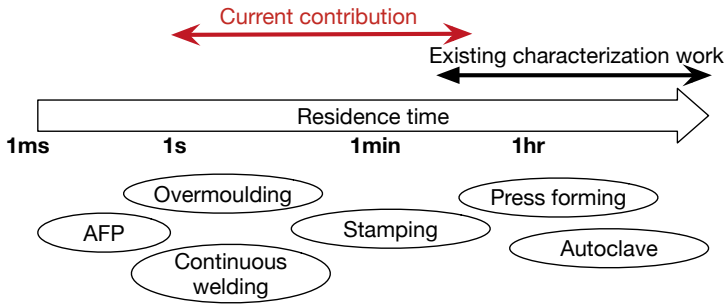

Figure 1: Many thermoplastic forming processes consist in short residence times at processing temperature. To our knowledge, however, there are no existing characterization methods for such short times.

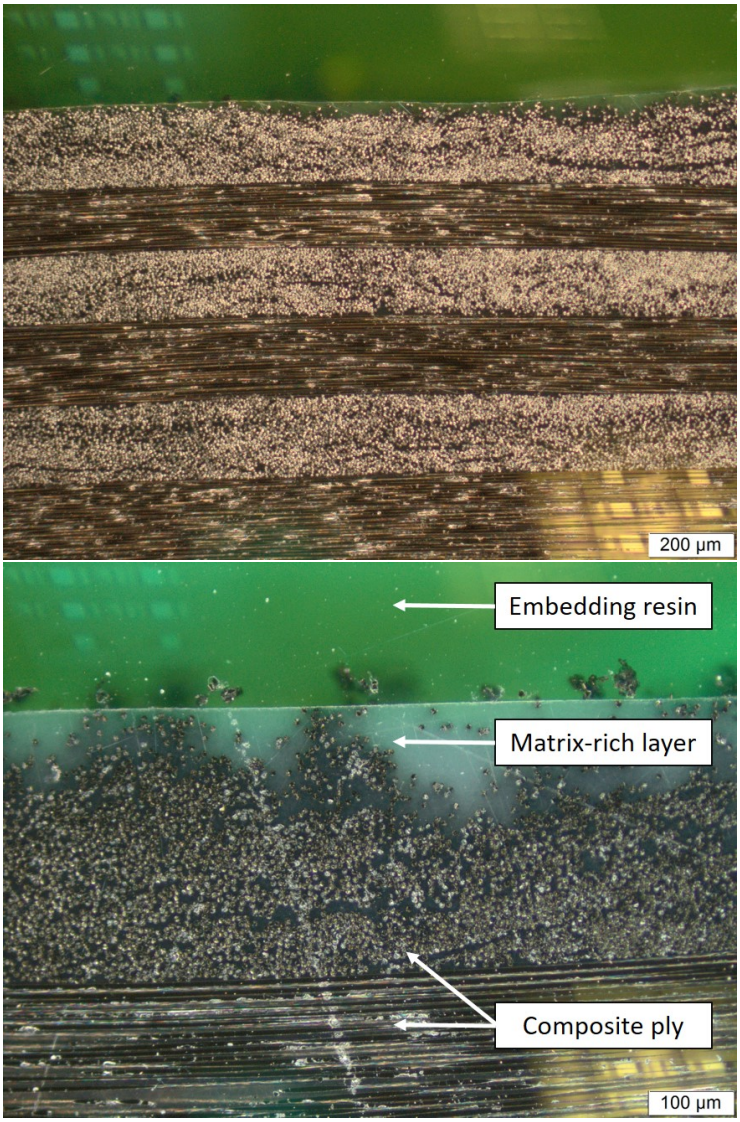

Figure 2: Cross-sectional micrographs of autoclave consolidated samples. The resin-rich layer is shown in the zoomed picture.

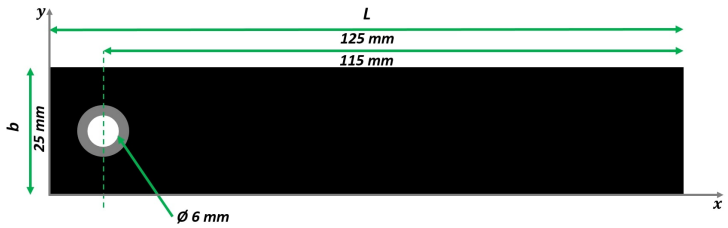

Figure 3: Dimensions of the composite coupons to be welded and tested with double cantilever beam tests. The grey circle represents the countersunk hole to insert the loading pin.

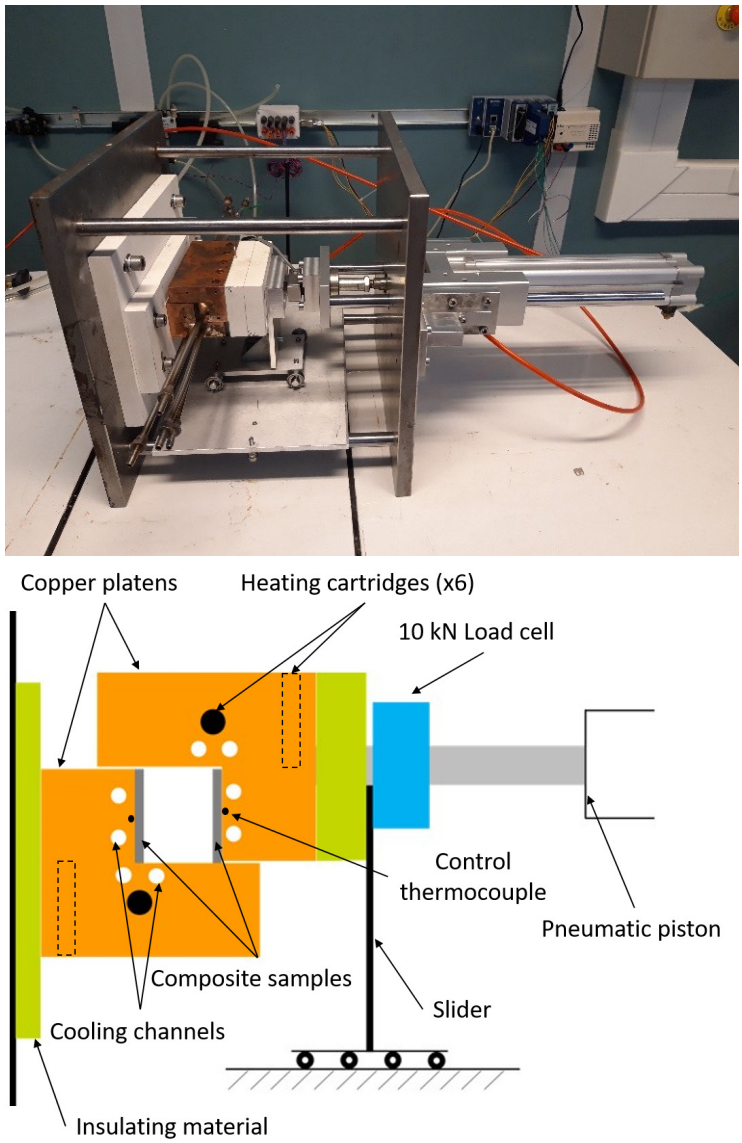

Figure 4: The experimental TACOMA setup, designed for welding under isothermal conditions followed by a fast cooling. (top): general view and (bottom): schematic view.

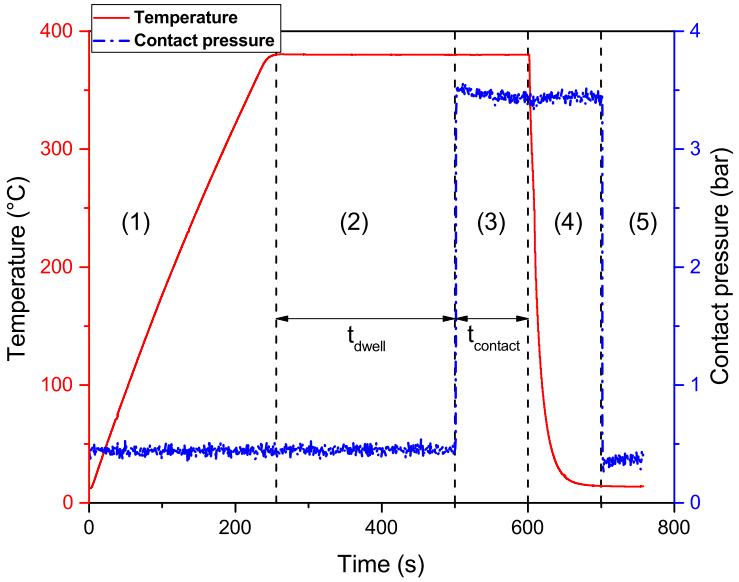

Figure 5: Experimental welding procedure. The heating (1) and temperature stabilization (2) occur before the samples are put in contact. The welding time is $t_{contact}$ (3) and quenching occurs in phase (4).

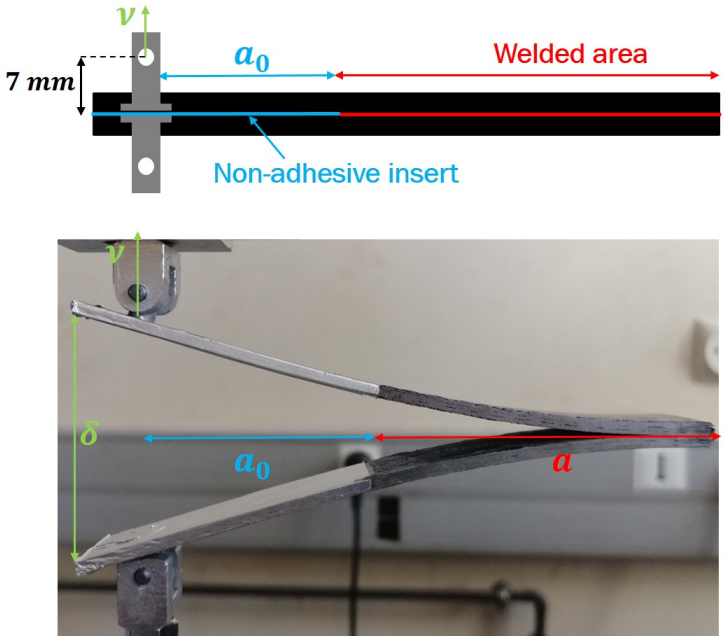

Figure 6: Double Cantilever Beam (DCB) setup. The initial crack length a_0 is known from the non-adhesive foil insert.

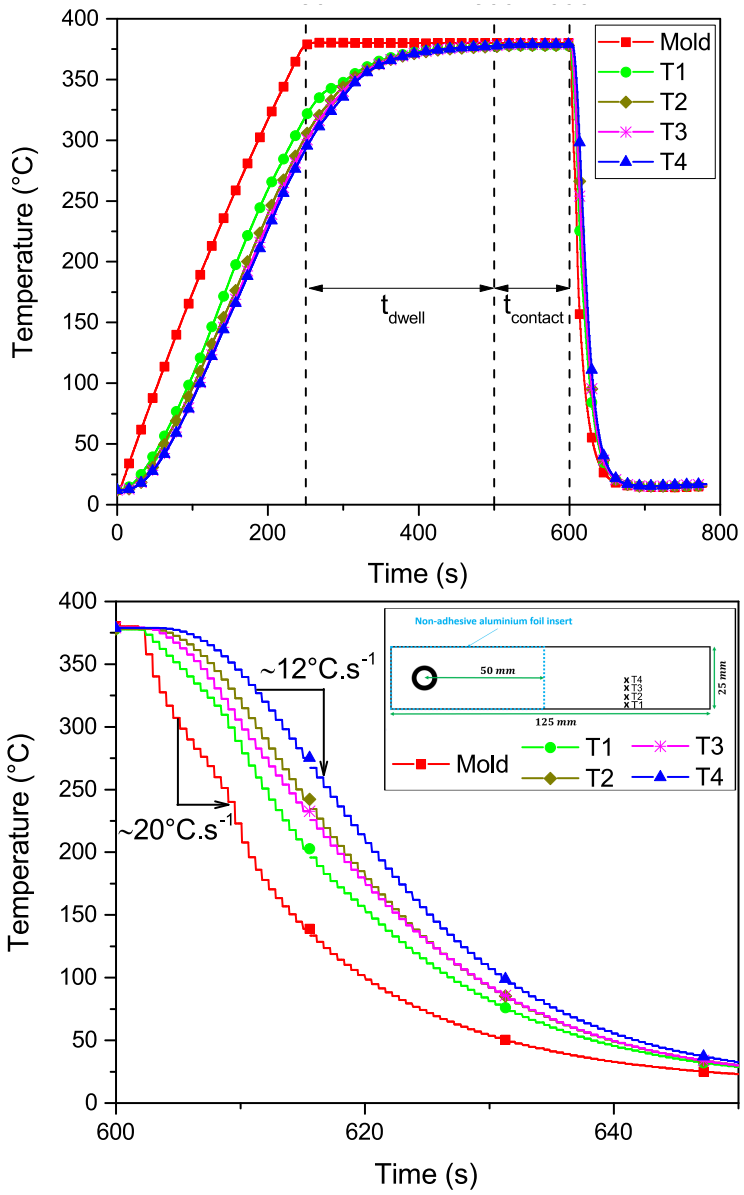

Figure 7: (Top) Temperature evolution according to time at different locations on the sample interfaces during the welding sequence; (Bottom) Close-up of the cooling phase.

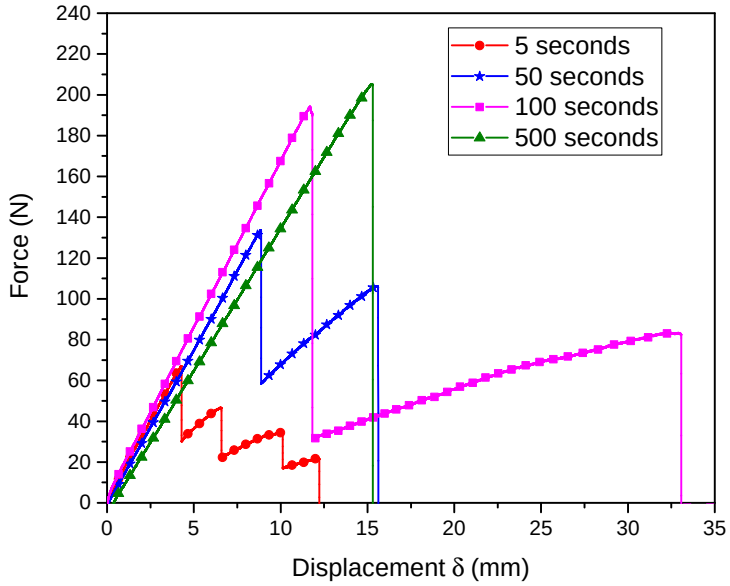

Figure 8: Load-displacement curves from the fracture double cantilever beam test corresponding to samples welded at 380°C for different contact times. Crack propagation is unstable, as observed by previous authors [33, 37].

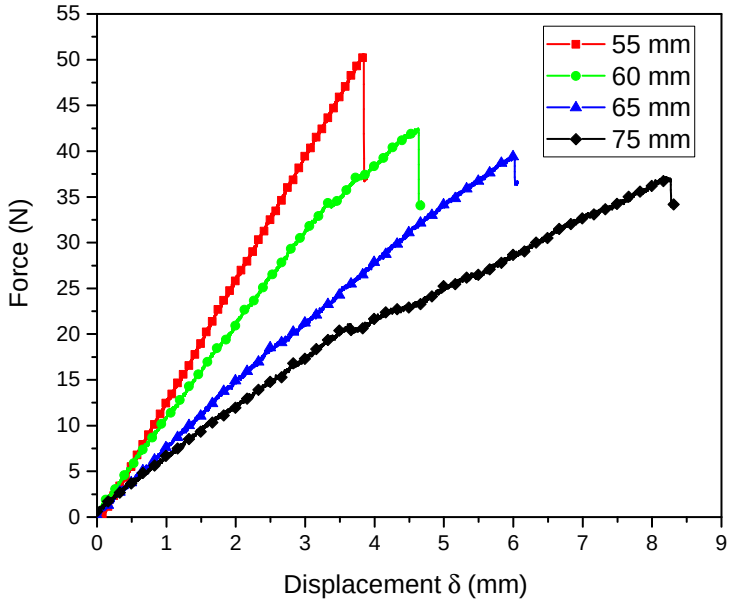

Figure 9: Load-Displacement curves using clamps positioned successively at different locations for 1 s contact time.

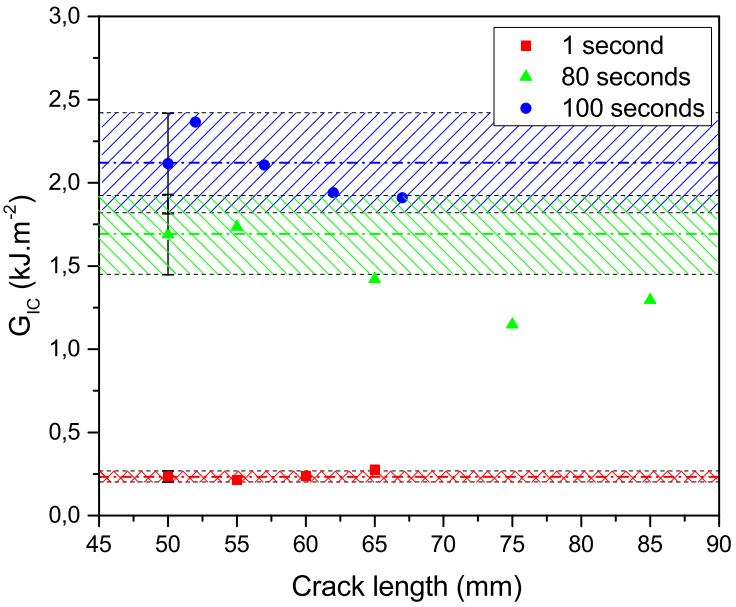

Figure 10: Interlaminar fracture toughness G_{IC} measured at different crack lengths from the incremental DCB fracture test. Samples were welded at 380°C for three different contact times. The hatched area corresponds to the standard deviation taken from the classical DCB test. The values for crack propagation all fall within this interval.

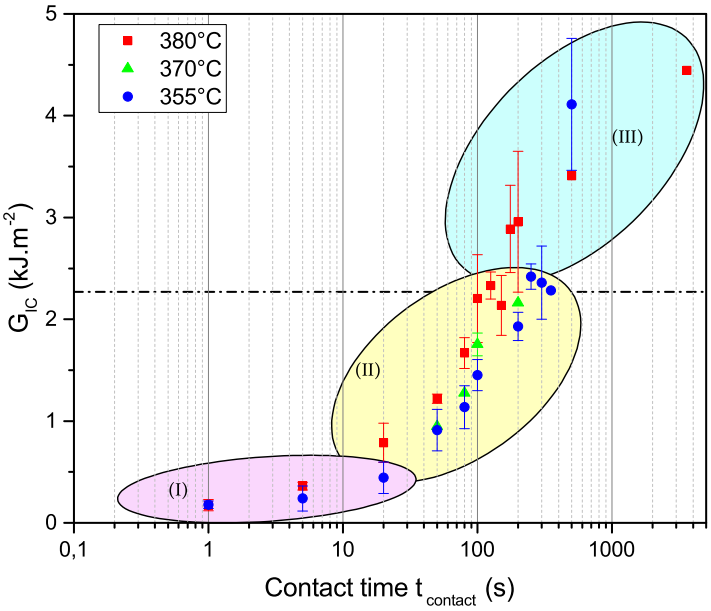

Figure 11: Interlaminar fracture toughness G_{Ic} plotted against contact time. Three regimes are identified: (i) a coupled regime where intimate contact is not fully achieved, (ii) a healing regime where the bonding energy increases with time and (iii) a terminal regime where other effects, such as fibre bridging, occur. The dotted line represents the maximum Interlaminar fracture toughness reached for the polymer healing stage.

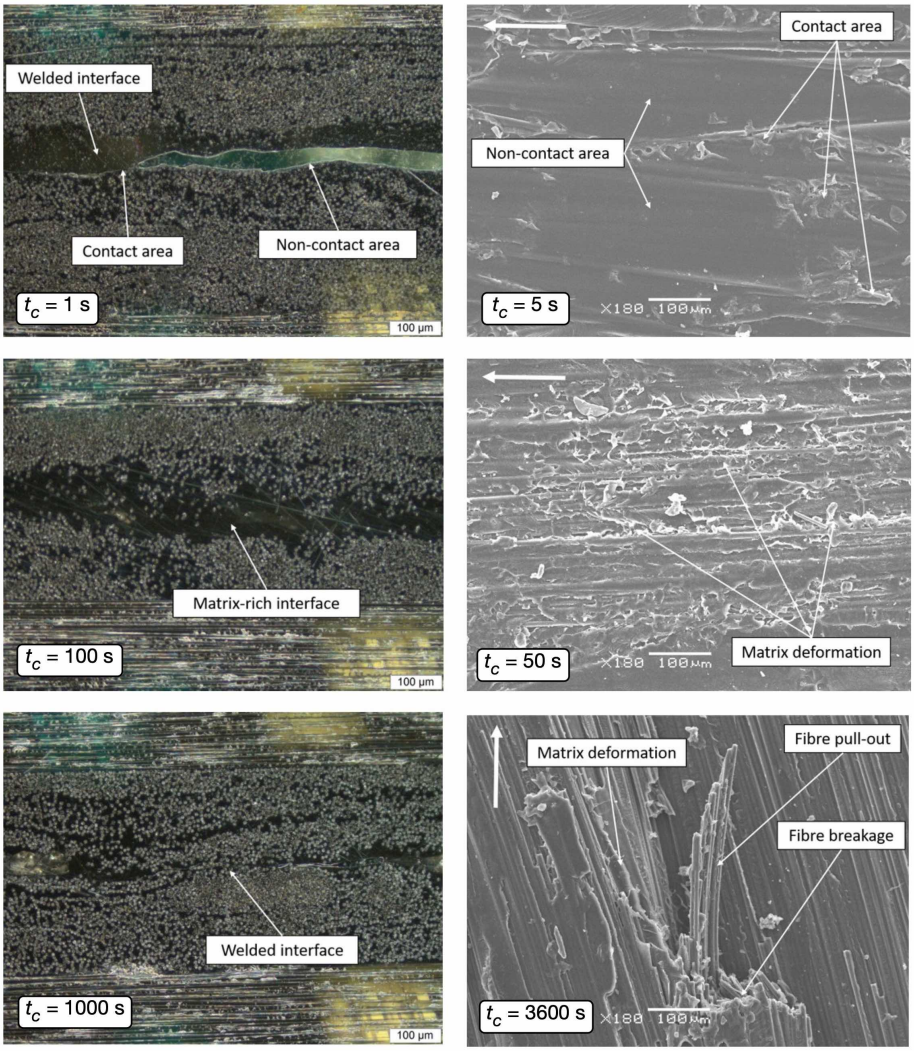

Figure 12: Cross-section optical micrographs (left) and SEM images of the fracture surfaces (right) of welded samples at 380°C under 3.2 bars with various residence time t_c. The arrow on the top left of the SEM images corresponds to the direction of crack propagation during the fracture test. Top: regime I with partial intimate contact, middle: regime II with a cohesive fracture of interfacial resin, and bottom: regime III with fibre bridging and pullout.

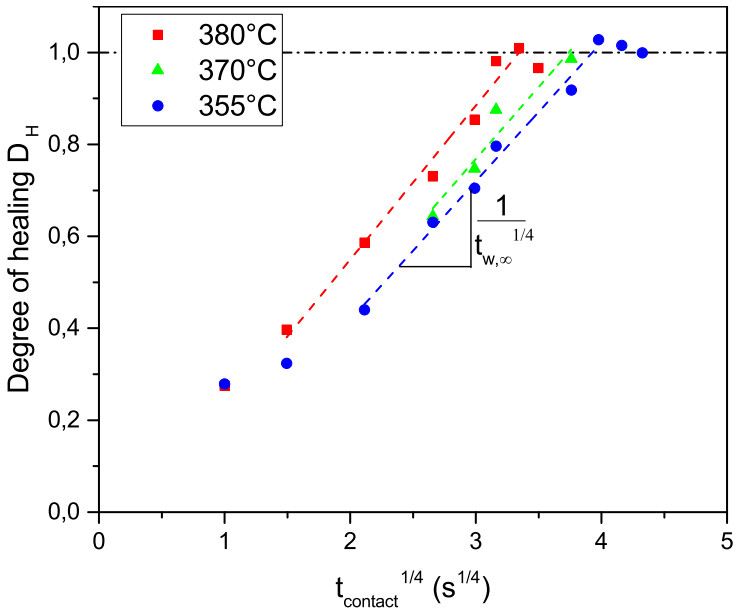

Figure 13: Degree of healing against the fourth root of contact time. The welding times are identified using the slope of the linear fit of the data corresponding to the second regime.

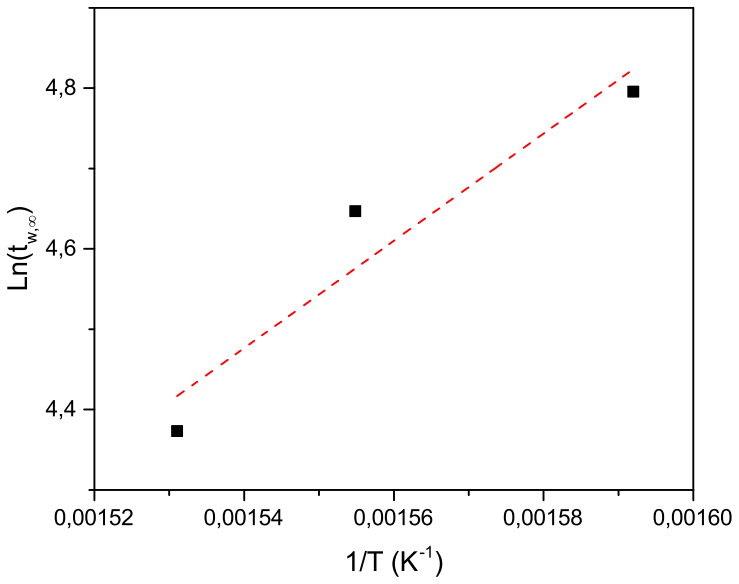

Figure 14: The obtained welding time $t_{w,\infty}$ is plotted against the inverse of the isothermal temperature $1/T$. This Arrhenius plot immediately identifies a temperature dependant law for welding time on temperature.

Table 1: Design of experiments. Number of replicates is indicated for each set of test conditions (isothermal temperature and contact time). Closing pressure is 3.2 bars for all tests.

$t_{contact}$ [s]	Temperature [°C]		
	355	370	380
1	3	/	3
5	4	/	3
20	3	/	3
50	3	1	3
80	3	1	4
100	3	2	8
125	/	/	4
150	/	/	3
175	/	/	3
200	3	1	4
250	3	/	/
300	3	/	/
350	1	/	/
500	2	/	1
3600	/	/	1
Total	76 experiments		

Table 2: Positions of the thermocouples on the interface of the instrumented samples. Axes are defined in Figure 3.

Thermocouple	T1	T2	T3	T4
Longitudinal distance along x (mm)	92.5	92.5	92.5	92.5
Transverse distance along y (mm)	2	5	8	12.5

Table 3: Identified welding times for the three isothermal temperatures.

Temperature (°C)	355	370	380
Welding time (s)	121	104	79